ELSEVIER

Journal of Membrane Science 208 (2002) 75–88

journal of MEMBRANE SCIENCE

www.elsevier.com/locate/memsci

Gas permeation in silicon-oxide/polymer (SiO_x/PET) barrier films: role of the oxide lattice, nano-defects and macro-defects

A.P. Roberts [a,*], B.M. Henry [a], A.P. Sutton [a], C.R.M. Grovenor [a], G.A.D. Briggs [a], T. Miyamoto [b], M. Kano [b], Y. Tsukahara [b], M. Yanaka [b]

[a] *Department of Materials, University of Oxford, Parks Rd, Oxford OX1 3PH, UK*
[b] *Toppan Printing Co. Ltd., Technical Research Institute, 4-2-3 Sugito-machi Takanodai-minami, Kitakatsushika-gun, Saitama 345-8507, Japan*

Received 10 December 2001; received in revised form 15 April 2002; accepted 22 April 2002

Abstract

We propose a model for permeation in oxide coated gas barrier films. The model accounts for diffusion through the amorphous oxide lattice, nano-defects within the lattice, and macro-defects. The presence of nano-defects indicate the oxide layer is more similar to a nano-porous solid (such as zeolite) than silica glass with respect to permeation properties. This explains why the permeability of oxide coated polymers is much greater, and the activation energy of permeation much lower, than values expected for polymers coated with glass. We have used the model to interpret permeability and activation energies measured for the inert gases (He, Ne and Ar) in evaporated SiO_x films of varying thickness (13–70 nm) coated on a polymer substrate. Atomic force and scanning electron microscopy were used to study the structure of the oxide layer. Although no defects could be detected by microscopy, the permeation data indicate that macro-defects (>1 nm), nano-defects (0.3–0.4 nm) and the lattice interstices (<0.3 nm) all contribute to the total permeation.

Keywords: Barrier films; Gas permeation; Diffusion pathways; Activation energy; Ceramic–polymer composites

1. Introduction

In the food packaging and medical device industries it is desirable to manufacture thin, flexible and transparent films which act as a barrier to oxygen and water vapour. To achieve this goal, one of the popular materials combinations is to deposit a thin layer (≈40 nm) of low-permeability silicon-oxide on a polymer substrate (12–25 μm) [1–3]. For oxygen, the permeance of these composite laminates is around 0.3–0.5 cm^3/m^2 per day under an applied pressure difference of 1 atm [1,2] which is surprisingly high. If the oxide-layer had a similar structure to silica glass [4,5] and contained no macroscopic defects (like cracks), the permeance would be expected to be lower by many orders of magnitude. This discrepancy indicates that to improve gas barrier composites it is crucial to understand the mechanism of gas permeation in the silicon-oxide layer, i.e. to clarify the major pathways of gas penetration through these layers. We address this question in this paper.

The fact that the permeation rate is so much higher than that expected for silica glass may indicate that the silicon-oxide contains defects or pinholes. This conclusion has been reached by other groups using either

* Corresponding author. Present address: Centre for Microscopy and Microanalysis, University of Queensland, Qld 4072, Australia.
E-mail address: Anthony.Roberts@mailbox.uq.edu.au (A.P. Roberts).

0376-7388/02/$ – see front matter
PII: S0376-7388(02)00178-3

Nomenclature

c	concentration (mol/cm^3)
C_{md}	geometric factor (Eq. (6))
D	diffusion coefficient (cm^2/s)
ΔE	activation Energy (kJ/mol)
j	flux (mol/(cm^2 s))
p	pressure (atm)
p.u.	permeation unit (10^{-18} mol/(cm s atm))
P	permeability (mol/(cm s atm))
R	gas constant (J/(K mol))
s	coefficient of solubility
S	solubility (mol/(cm^3 atm))
T	temperature (K)
ϕ	volume fraction

Subscripts

b	barrier-film
g	glass (oxide)
ILT	ideal laminate theory
la	lattice
md	macro-defects
nd	nano-defects
p	polymer

measurements of the activation energy of permeation [2] or microstructural studies [3]. In this picture, no gas flux passes through the oxide directly, instead passing through the postulated defects. Recently, however, evidence has been found that gas is permeating through the oxide itself [6]. Nevertheless, the O_2 and H_2O permeation is still many orders of magnitude greater than would be expected if the oxide layer had a structure similar to silica glass. Moreover, the measured activation energy for permeation is around half that previously measured for silica glass. Characterisation studies have yielded little information about the lattice structure of SiO_x, and it is possibly quite different to annealed silica glass. The permeation data referred to above indicate a more open structure.

In this paper, we propose a model for inferring the structure of the deposited SiO_x material from permeation measurements. An earlier version of our model has been employed by other groups in this manner [6], and it is timely to provide the details. Furthermore, in the future, the concentration of macro-defects in barrier films are likely to be further minimised, and it is important to construct a model describing permeation through the nano-porous oxide layer.

We propose gas and water vapour transport in gas barrier films is comprised of contributions from three components: un-hindered transport through 'macro-defects' (>1 nm) in the oxide layer, hindered transport through 'nano-defects' (<1 nm), and hindered transport through the amorphous lattice of the oxide (interstice < 0.3 nm). A schematic is shown in Fig. 1. The relative contribution of each component depends on the size of the permeant molecule (or atom), and the number and size of each class of defect.

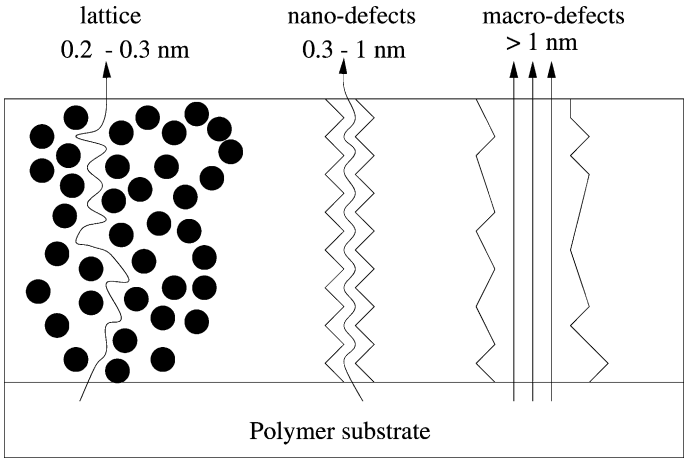

Fig. 1. A schematic diagram showing the proposed gas transport pathways through the oxide layer. The relative importance of each path depends on gas permeant size.

Note that our specification of 'macro-defects' is based on the defect size being three or four times as large as a typical permeant atom/molecule (0.2–0.3 nm). In this case, the defect will provide little resistance to gas flux. For example, boundaries between grain-like structures observed in SiO_x coatings [7] would correspond to macro-defects or nano-defects depending on whether they were larger or smaller than 1 nm.

We have measured the permeation of helium, neon and argon in barrier films with varying coating thickness of SiO_x. The polymer substrate is poly(ethylene terephtalate) (PET). The use of inert gases is desirable because it precludes any interaction between the material and permeant. Moreover, the variation of atomic radius between the gases allows additional microstructural information to be collected. The interpretation of the data in terms of the model allows us to determine the relative permeation through each of the three suggested pathways, and estimate the size distribution of defects.

2. Theory

2.1. Permeability, diffusion and solubility

In the literature of barrier films, the oxygen flux is usually reported in cm^3/m^2 per day and the water vapour flux in g/m^2 per day. In order to discuss the properties of barrier film materials it is important to convert the units of flux into intrinsic material properties (such as permeability, diffusion coefficient and solubility), which are discussed extensively in the wider literature [8–10]. Since the units in which these quantities are reported differ widely amongst fields, and are somewhat complicated, we provide a brief discussion below.

The diffusion coefficient D (usually reported in cm^2/s) is defined as the ratio of molar flux to the concentration gradient $D = -j\,\Delta x/\Delta c$. For gases, it is generally easier to measure the pressure differential across the film giving rise to a permeability coefficient $P = -j\,\Delta x/\Delta p$. For the gases considered here (excluding water vapour) the concentration at the surface (or throughout the solid in equilibrium) is proportional to the pressure (Henry's law) $c = Sp$ where S is the solubility, so that $P = DS$. If c has units of mol/cm^3 and p is measured in atm then S has units of $mol/(cm^3\,atm)$ and P has units of mol/(s cm atm).

Since an independent experiment must be carried out to measure the solubility it is useful to have rough estimates of S in order to relate diffusion coefficients published in the literature to gas barrier permeability measurements. The dimensionless 'coefficient of solubility' s (defined as the ratio of the concentration of gas dissolved in the glass to the concentration of molecules in the gas phase) has been found to have a constant value of $s = 0.02$ for He, Ne and $s = 0.01$ for Ar over the temperature range $T = 0$–$1000\,^\circ C$ in fused silica [11]. The simplest explanation of this observation is that s directly measures the volume fraction of the solid accessible to gas atoms (the fraction being less for larger argon atoms) [11]. The solubility S is related to s by:

$$S = \frac{T_{\mathrm{std}}}{T} s c_{\mathrm{std}} \tag{1}$$

Here, $c_{\mathrm{std}} = 4.03 \times 10^{-5}\ mol/cm^3$ is the concentration of atoms in the gas phase at standard temperature and pressure ($T = 298\,^\circ C$ and $p = 1$ atm). Given that $s \approx 0.015$ is nearly constant, and the temperature range we consider is small, for simplicity we assume the solubility is constant with value $S = 0.015 \times c_{\mathrm{std}} \approx 60 \times 10^{-8}\ mol/cm^3$.

Since water vapour flux is not driven by a pressure gradient, it is generally characterised by a diffusion coefficient. However, for our purposes it is useful to use a fictitious water permeability in units which, under standard gas barrier conditions (1 atm for inert gases and oxygen, 100% RH for water vapour), would give an equivalent molar flux if the numerical values of the gas permeability and fictitious water vapour permeability were identical. To this end, we define the fictitious water vapour permeability as $P = Dc_w$ with D given in cm^2/s, and c_w the concentration of water (mol/cm^3) in the oxide surface. The units of P are then mol/(s cm). The 'solubility' c_w of water in silica glass at 200 °C has been estimated to be ≈500 ppm by weight [12]. Assuming the density of glass is $2.2\ g/cm^3$ this gives $c_w = 5 \times 10^{-4} \times 2.2\ g/cm^3 \times 1/18\ mol/g = 6.1 \times 10^{-5}\ mol/cm^3$. In rhyolitic glasses (77% SiO_2) [13], the solubility is around 0.3% (by weight) giving $c_w = 3.7 \times 10^{-4}\ mol/cm^3$. For simplicity we adopt an intermediate value $c_w = 1 \times 10^{-5}\ mol/cm^3$.

For a 12 μm thick barrier (a standard thickness of PET film), a gas transmission rate of 1 cm^3/m^2 per day/atm ×12 μm corresponds to 56×10^{-18} mol/(cm s atm) = 56 p.u. where for simplicity we have defined 1 permeation unit (p.u.) as 10^{-18} mol/(cm s atm) (for oxygen or the inert gases). For the same thickness of polymer film, a water vapour flux of 1 g/m^2 per day ×12 μm corresponds to a fictitious permeability of 0.16×10^{-12} mol/(cm s) = 160 kp.u. where, for water vapour, 1 p.u. is 10^{-18} mol/(cm s).

2.2. Ideal laminates and macro-defects

Assuming that the ceramic layer is macro-defect free and homogeneous, the permeability P of a barrier film (thickness d) is given by ideal laminate theory (ILT) as [1,14,2]:

$$P_{\mathrm{ILT}} = \left(\frac{\phi_\mathrm{p}}{P_\mathrm{p}} + \frac{\phi_\mathrm{g}}{P_\mathrm{g}}\right)^{-1}, \quad \phi_\mathrm{p} = d_\mathrm{p}/d, \quad \phi_\mathrm{g} = \mathrm{d_g}/d \tag{2}$$

where d_p, ϕ_p and P_p are the thickness, volume fraction and permeability of the polymer substrate and d_g, ϕ_g and P_g are the values for the glass layer ($d_\mathrm{p} + d_\mathrm{g} = d$, $\phi_\mathrm{p} + \phi_\mathrm{g} = 1$). If $P_\mathrm{g}/\phi_\mathrm{g} \ll P_\mathrm{p}/\phi_\mathrm{p}$ then by Eq. (2):

$$P_\mathrm{b} = P_{\mathrm{ILT}} \approx \frac{P_\mathrm{g}}{\phi_\mathrm{g}} \tag{3}$$

where we have put P_b, the permeability of the composite barrier, equal to P_{ILT}. If the film is an ideal laminate structure we can estimate the permeability of glass from measurements of P_p and P_b as:

$$P_\mathrm{g} = \phi_\mathrm{g}\left(\frac{1}{P_\mathrm{b}} - \frac{\phi_\mathrm{p}}{P_\mathrm{p}}\right)^{-1} \approx \phi_\mathrm{g} P_\mathrm{b} \tag{4}$$

The stated approximation holds for standard composite barriers (40 nm thick oxide layer and 12 μm thick polymer substrate, so $\phi_\mathrm{p} \approx 1$) if $P_\mathrm{b} \ll P_\mathrm{p}$.

In the case where the oxide layer has macro-defects (>1 nm) we model the permeability as:

$$P_\mathrm{b} = P_\mathrm{md} + \left(1 - \frac{P_\mathrm{md}}{P_\mathrm{p}}\right) P_{\mathrm{ILT}} \tag{5}$$

where P_md is the permeability of the defects assuming that the permeability of the oxide layer is negligible (i.e. $P_{\mathrm{ILT}} = 0$). Eq. (5) is based on extensive numerical solution of the partial differential equation for diffusion [15]. The factor $(1 - P_\mathrm{md}/P_\mathrm{p}) < 1$ reflects the fact that permeation through the glass/polymer layer is reduced (below P_{ILT}) by the presence of macro-defects. It has been shown [14,16] that the macro-defect permeability is directly proportional to the polymer permeability, $P_\mathrm{md} = C_\mathrm{md} P_\mathrm{p}$, where C_md is a dimensionless constant which depends on the size and number of macro-defects in the film. Note that if the oxide layer is practically impermeable ($P_\mathrm{g} = 0$) then $P_{\mathrm{ILT}} = 0$, and Eq. (5) gives

$$P_\mathrm{b} \approx C_\mathrm{md} P_\mathrm{p} \tag{6}$$

The actual form of C_md has been given for circular holes [14] and rectangular holes (including cracks) [16]. For an oxide layer with periodically repeated (spacing L) rectangular macro-defects of size $2w \times 2h$ deposited on a substrate of depth d:

$$C_\mathrm{md} \approx 2\pi \frac{\sqrt{wh}d}{L^2}\left(H\left(\frac{h}{w}\right) - \frac{\sqrt{wh}}{d}\ln 2\right)^{-1} \tag{7}$$

with

$$H(s) = s^{-1/2}\ln\left(\sqrt{1+s^2} + s\right) - s^{1/2}\ln\left(\sqrt{1+s^{-2}} - s^{-1}\right)$$

The approximation holds for $w, h \ll d \ll L$. More general results for all w, h and d, and a result for the case of cracks, are given in [16]. Importantly, C_md is a geometric constant that is independent of both temperature and permeant species.

The temperature dependence of the diffusion coefficient for molecules in solids (e.g. glass [17,18]) and polymers [19] is generally given by an Arrhenius law:

$$D = D^\infty \exp\left(-\frac{\Delta E}{RT}\right) \tag{8}$$

the energy of activation ΔE being related to the energy necessary for the molecule to squeeze through the lattice interstices. Since the solubility is linear in T and the temperature range over which barrier films are studied is small (10 °C ≤ T ≤ 60 °C), the activation energy of permeation is expected to be identical to that of diffusion.

Ideal laminate theory, and the macro-defect theory, provide the basis for a key test to determine the presence of macro-defects [2]. First, if the oxide layer has no defects, then it is expected to have an extremely low permeability, and Eq. (3) shows that the barrier

permeability is directly proportional to the oxide permeability. Therefore, if the activation energy of the barrier layer is equivalent to the expected activation energy of oxide (100 kJ/mol for O_2 in vitreous silica [4]) the barrier is macro-defect free. Note that activation energy of the barrier film is not the sum of the activation energies of the substrate and oxide layer (see Eq. (3)). On the other hand, if the oxide layer contains macro-defects, but is otherwise practically impermeable, the barrier permeability will be directly proportional to the polymer permeability by Eq. (6), and the activation energy of the barrier will be equivalent to the activation energy of permeation through the polymer (typically around 35 kJ/mol for O_2) [20]. In between these limiting cases (defect or oxide dominated) the barrier does not have a true activation energy, but over a small temperature range it will show an apparent activation energy between the two limits $\Delta E_p < \Delta E_b < \Delta E_g$ (if $\Delta E_p < \Delta E_g$).

The assumed large difference in the activation energies of defect-free oxide and the polymer substrate (it is thought that $\Delta E_g \gg \Delta E_p$) allows a clear statement to be made about the presence of defects depending on whether $\Delta E_b \approx \Delta E_p$ or $\Delta E_b \approx \Delta E_g$. A key problem with this approach is that P_g and ΔE_g are not precisely known since no study has detected H_2O or O_2 permeation through silica glass at room temperature. Certainly, if high temperature results are extrapolated to $T = 25\,^\circ$C, no permeation would be detectable even for the extremely thin oxide layers of barrier films. But such an extrapolation may not be justified. For example, in silica above 400 °C, Barrer [8] found $\Delta E_g(H_2) = 45$ kJ/mol, but at 193 °C the activation energy of permeation was reduced to $\Delta E_g(H_2) = 18$ kJ/mol. A qualitatively similar change in the temperature dependence of argon, nitrogen and air permeation at low temperatures was observed. This was attributed to presence of 'faults and cracks of molecular dimensions', which we call nano-defects (<1 nm).

2.3. Nano-defects

If nano-defects are present in the oxide lattice, we model the effective permeability of the glass as:

$$P_g = P_{la} + P_{nd} = P_{la}^{\infty} \exp\left(\frac{-\Delta E_{la}}{RT}\right) + P_{nd}^{\infty} \exp\left(\frac{-\Delta E_{nd}}{RT}\right) \quad (9)$$

where the subscript 'la' corresponds to the amorphous lattice, and 'nd' corresponds to the nano-defects. Note that Eq. (9) assumes the glass layer has an 'effective' permeability. This is tantamount to assuming an isolated layer (i.e. not deposited on a substrate) of the glass provides a finite resistance to gas flow. In contrast, macro-defects provide no resistance, and their effect is modelled instead by Eq. (5).

Since the nano-defects are larger than the interstices in the lattice $\Delta E_{nd} < \Delta E_{la}$. At high temperatures both pathways contribute, but the lattice component dominates, because the nano-defects are rarer than lattice interstices. This implies that in fused silica, high temperature (e.g. $T > 500\,^\circ$C) estimates of ΔE_g are really measurements of ΔE_{la}. At low temperatures, the large activation energy of lattice diffusion kills off the lattice contribution leaving only the nano-defect contribution [8]. It is possible that similar nano-defects play a role in barrier permeation, since the method of depositing SiO_x on polymer films is significantly different to the manufacture of silica glass, which is generally annealed at high temperatures. The distribution of nano-defects in the barrier layers might, therefore, be expected to differ considerably from silica glass, and the permeation properties of these barriers are usually measured closer to room temperature where nano-defects may dominate transport.

The model given above may also explain the anomalous [12] temperature dependence of water diffusion in silica glass. For $T > 550\,^\circ$C the authors reported $\Delta E_g \approx 80$ kJ/mol, while for $T < 550\,^\circ$C an activation energy of $\Delta E_g \approx 40$ kJ/mol was found [12]. Therefore, the interpretation of gas barrier permeabilities in terms of activation energy must be undertaken carefully. There are a number of instances in the literature [6,7], and we will show more, where $\Delta E_b > \Delta E_p$, but the values are not sufficiently high to warrant identification as the oxide lattice activation energy ΔE_{la}. We argue instead that the activation energy is related to hindered diffusion through nano-defects. Since the role of nano-defects in glass are not well understood, we now discuss their contribution to permeation.

The simplest way to estimate the contribution of nano-defects to permeation in barrier films is to examine the permeation/diffusion properties of solids with larger pore sizes (or lattice interstices) than those of silica glass. Shelekhin et al. [21] have studied gas permeation in 'micro-porous' glass (with pore windows

of around 0.6 nm). A modified Knudsen formula [22] was necessary to describe the data (particularly for helium)

$$P = d_p \sqrt{\frac{8}{\pi MRT}} \frac{\phi}{3\tau} e^{-\Delta E/RT} \quad (10)$$

here d_p is the pore diameter, M the molecular weight, ϕ the porosity and τ a tortuosity factor. Over the temperature range relevant to gas barrier films the factor of $T^{-1/2}$ can be effectively ignored (as we have done for the solubility which increases in proportion to T). For large 'pore' sizes the permeation no longer follows an Arrhenius law, instead diffusion is limited by collisions with pore walls (Knudsen diffusion). Intermediate behaviour (between Knudsen and hindered diffusion) was observed by Lord Rayleigh for a 1 nm wide planar pore (e.g. see [8]). This specifies our upper limit for nano-defects.

We report the activation energy of permeability and the absolute permeability of several well characterised solids in Table 1. This provides a 'scale' with which data for barrier films can be compared [21]. The

Table 1
The permeability (units 10^{-18}mol/(cm s atm)) and activation energy (kJ/mol) of permeation for glasses and micro-porous solids previously studied in the literature

Material	Gas	P	ΔE	D	S	T (°C)	P (30 °C)	D (30 °C)	Reference
Annealed silicon oxide (0.27 nm)	He	1.7E+04	22			25	2.0E+04		[18]
	Ne	4.0e + 01	38	0.58	69	79	4.7E+00		
	Ar	2.2E+00	105	0.16	14	644	8.9E−13		
Zeolite KA (0.3 nm)	Ne		29	2.9E−03		20	2.6E−01[a]	4.3E−03	[24]
	Ar		53	1.6E−07		20	2.0E−05[a]	3.3E−07	
K-mordenite (≈0.4 nm)	Ar		35	2.4E−06		−78	3.8E−01[a]	6.3E−03	[24]
	O_2		18.4	2E−05		−78	7.5E−02[a]	1.3E−03	
Micro-porous glass (0.6 nm)	He	2.8E+09[b]	0.5			25	2.8E+09		[21]
	O_2	3.1E+06[b]	12			25	3.3E+06		
Vitreous silica (0.27 nm)	O_2	2.8E+02	92			900	2.6E−10		[4]
Soda-lime glass (<0.27 nm)	He	2.3E+00	46			25	3.1E+00		[17]
Silica glass	H_2O		80	1.0		730	1.4E−07[c]	1.4E−10	[12]
	H_2O		40	1.0E−03		200	2.9E−03[c]	2.9E−06	
Isotropic PET	O_2	1.6E+04	34[d]			25	2.0E+04		[20]
Crystalline PET	O_2	8.4E+03	35[d]			25	1.1E+04		[20]
Isotropic polyethylene	He	6.4E+05				25			[25]
	O_2	3.5E+05				25			
Crystalline polyethylene	He	6.2E+04				25			[25]
	O_2	9.7E+03				25			
Glassy PET	He		20						[19]
	O_2		46						
Rubbery PET	He		28						[19]
	O_2		51						
PET	O_2				250				[26]

The solubility is given in units of 10^{-8} mol/cm^3, and the diffusion coefficient in units of 10^{-10} cm^2/s. The data in columns 3–6 is taken directly from the source (except where noted). The data in columns 8 and 9 is extrapolated from the source data using Arrhenius' law.

[a] Estimated using $P = SD$ with $S = 60 \times 10^{-8}$ mol/cm^3 (see text).

[b] Estimated using $P = SD$ with $S = 1000 \times 10^{-8}$ mol/cm^3 (see text).

[c] P estimated from Fig. 7 in [21].

[d] Estimated from P reported at 25 and 60 °C.

Table 2
The diameter of various gases discussed in this paper (after Doremus [11])

Gas	Diameter (nm)
He	0.20
Ne	0.24
Ar	0.32
O_2	0.32
H_2O	0.33

degree to which such comparisons can be made between materials of different chemical structure is of course limited, nevertheless, the data provide a useful benchmark. For reference, we also report literature values of P and ΔE for polymers.

There are several obvious trends in the data. In a given material ΔE increases with kinetic diameter of the permeant molecule (Table 2). This is attributed to the greater energy required by a molecule to 'squeeze' through a pore-window. For tightly packed glasses a square law (i.e. $\Delta E \propto (\text{radius})^2$) has been proposed [18,11]. For a fixed permeant molecule (e.g. He) ΔE falls extremely rapidly with increasing pore size. For example $\Delta E = 46$ kJ/mol for He in dense soda lime glass (pore size <0.27 nm) and $\Delta E = 0.5$ kJ/mol for micro-porous glass (pore size 0.6 nm). A crucial implication from the table is that a small increase (10%) in pore size can halve the activation energy of permeation. For example, an increase in 'pore' size from 0.27 to 0.3 nm reduces the activation energy of argon permeation from 105 to 53 kJ/mol.

In general, we expect that as ΔE increases P will decrease, since the diameter of the pore channels is decreasing. But this need not be true. The permeability also depends on the number of channels (represented by the porosity ϕ in Eq. (10)). This may explain why neon diffusion is unexpectedly lower in zeolite (0.3 nm pores, $\Delta E = 29$ kJ/mol) than silicon oxide (0.27 nm pores, $\Delta E = 29$ kJ/mol).

2.4. Implications for experiments on barrier films

Combining Eqs. (2), (5) and (9) we propose that gas and water vapour permeation in barrier films can be described by the formula:

$$P_b = C_{md} P_p + \left(\frac{\phi_p}{P_p} + \frac{\phi_g}{P_{la} + P_{nd}} \right)^{-1} \quad (11)$$

where $P_p = P_p^\infty \exp(-\Delta E_p/RT)$, $P_{la} = P_{la}^\infty \exp(-\Delta E_{la}/RT)$ and $P_{nd} = P_{nd}^\infty \exp(-\Delta E_{nd}/RT)$ are, respectively, the permeabilities of the polymer substrate, nano-defect free lattice, and nano-defects.

The factor $(1 - P_{md}/P_p)$ appearing in Eq. (5) has been replaced by unity since $C_{md} < 0.05$ in the barrier films we consider. The physical picture underlying the model is shown in Fig. 1. The relative importance of each term will depend on its magnitude and the geometric factors (ϕ_p, ϕ_g and C_{md}).

The activation energy test for determining the presence of macro-defects may be confounded by anomalously low activation energies arising from nano-defects in the oxide layer (i.e. ΔE_g and ΔE_p may be similar in magnitude). Moreover, at room temperature, the presence of nano-defects will also significantly increase the magnitude of the permeability above values extrapolated from high temperature experiments. This may also invalidate the activation energy test, since the hypothesis that $P_g/\phi_g \ll P_p/\phi_p$ (recall $\phi_g \ll \phi_p$) upon which Eq. (3) is based, may no longer be true. Therefore, it would be useful to have a complimentary test for macro-defect dominated permeation. If $P_g = P_{la} + P_{nd} \approx 0$ then, from Eq. (6), the ratio $P_b/P_p = C_{md}$ should be independent of temperature (which gives the same information as the activation energy test), but also independent of the permeant gas. As a consistency check it is possible to infer some geometric properties of the defects if C_{md} is known from Eq. (7). A third useful interpretative quantity is P_g, the permeability of the glass. This can be calculated from Eqs. (4) and (5) if macro-defects are present. If the properties of the glass layer do not vary with deposited thickness, this value should be independent of thickness. In addition to the activation energy of permeation, the absolute value of P_g can be useful for inferring the 'pore' scale (of the lattice interstices or nano-defects) by comparison with the data presented in Table 1.

3. Experimental details

3.1. Materials

We used a roll-to-roll vacuum deposition coater to produce SiO_x films of varying thickness (13–67 nm). A schematic cross-sectional diagram of the instrument

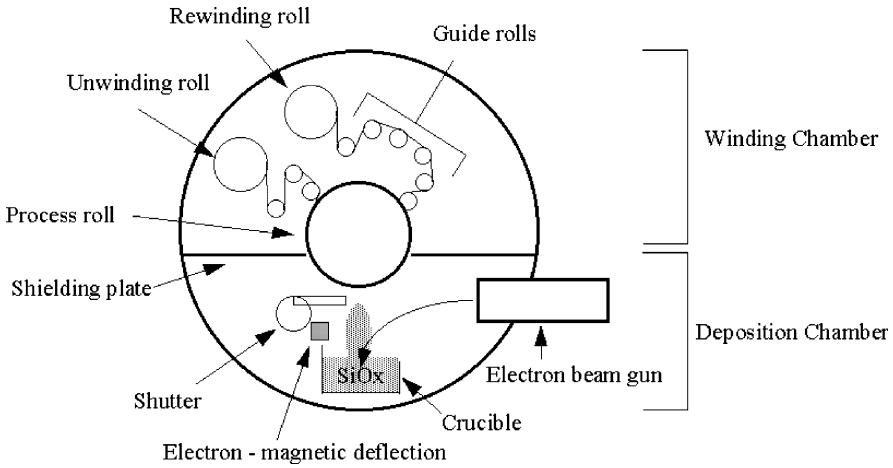

Fig. 2. Schematic diagram of the roll-to-roll vacuum deposition coater.

is shown in Fig. 2. The vacuum chamber of the machine was divided into a 'winding' and 'deposition' chamber by a shielding plate and cooled processing role. The upper-section contains guide rolls for film un-winding and rewinding. In the lower section, an electron beam gun (guided by an electro-magnetic deflection coil) is used to evaporate the raw Si–O material from a water-cooled copper crucible. To avoid film damage by the splash of un-vaporised hot materials, the deposition speeds were maintained at about 500 nm/s by a stable power of 16 kW (30 kV, 0.53 A). The base material was a PET film (Toray Co. Ltd., P-60:12 μm) and the SiO_x coating thickness was controlled by varying the roll-to-roll speed from 0.5 to 6.0 m/s. The reported thickness of the SiO_x layers was measured by an X-ray fluorescence meter which had been calibrated by transmission electron microscopy.

The surface morphology of the evaporated SiO_x ($x \approx 1.7$) coating was examined using the techniques of scanning electron microscopy (SEM) and atomic force microscopy (AFM). A JSM 840f scanning electron microscope operated at 1 kV accelerating voltage was used to investigate the coating in the absence of any deposited conducting film. A special SEM stage was constructed to allow 40 mm × 40 mm areas of each sample to be examined. Using precisely the same areas for gas permeation and microstructure measurements ensured that a one-to-one correlation could be made between the microstructure and permeation measurements. For AFM studies a Park SFM BD2 atomic force microscope was used.

3.2. Permeation measurements

The permeabilities of inert gases (He, Ne and Ar) were measured using the Gas Permeation Measurement System of Yanaco Analytical Instruments Co. (GTR-30XT). The sample film divides the measurement cell into two sections. The upper half is filled with the permeant gas at a pre-set pressure (2 atm), while the lower half is evacuated (the pressure difference providing the driving force of permeation). The gas that penetrates the film during a given time period is collected and flushed by a carrier gas to a chromatograph detector. Measurements of the permeability at different temperatures (30, 45 and 60 °C) allowed us to estimate the activation energy of permeation.

The oxygen permeability was measured using an OXTRAN instrument (Mocon Co., 10/50A). In this case, the upper half of the cell is maintained at 1 atm pressure of O_2 and the lower half at 1 atm pressure of N_2. The temperature (30 °C) and humidity (70% RH) of the cell were held constant. In contrast to the instrument used for inert gases, the driving force of permeation is the partial pressure of O_2. The volume of O_2 collected in a given time is measured by a nickel–cadmium sensor.

3.3. Characterisation

Microstructural characterisation of the barrier layer is crucial in order to establish the possible presence of pores and pinholes that would otherwise dominate permeation. Scanning electron and atomic force microscopes were used to investigate the structural integrity of the evaporated SiO_x coatings. Extensive SEM examination of the barrier coatings revealed no obvious pinholes or macro-scale defects in the structures.

Fig. 3 shows AFM images of the 13 and 43 nm SiO_x layers. These images indicate an irregular surface array of columnar grain-like structures similar to those reported by Tropsha and Harvey [2]. Chemical removal of the barrier layer revealed that the underlying PET surface is smooth. This observation supports the hypothesis that the SiO_x surface roughness is linked to growth around isolated nucleation centres.

Altogether, the SEM and AFM investigations show that all the coatings were uniform; including the 13 nm coating which completely covered the PET.

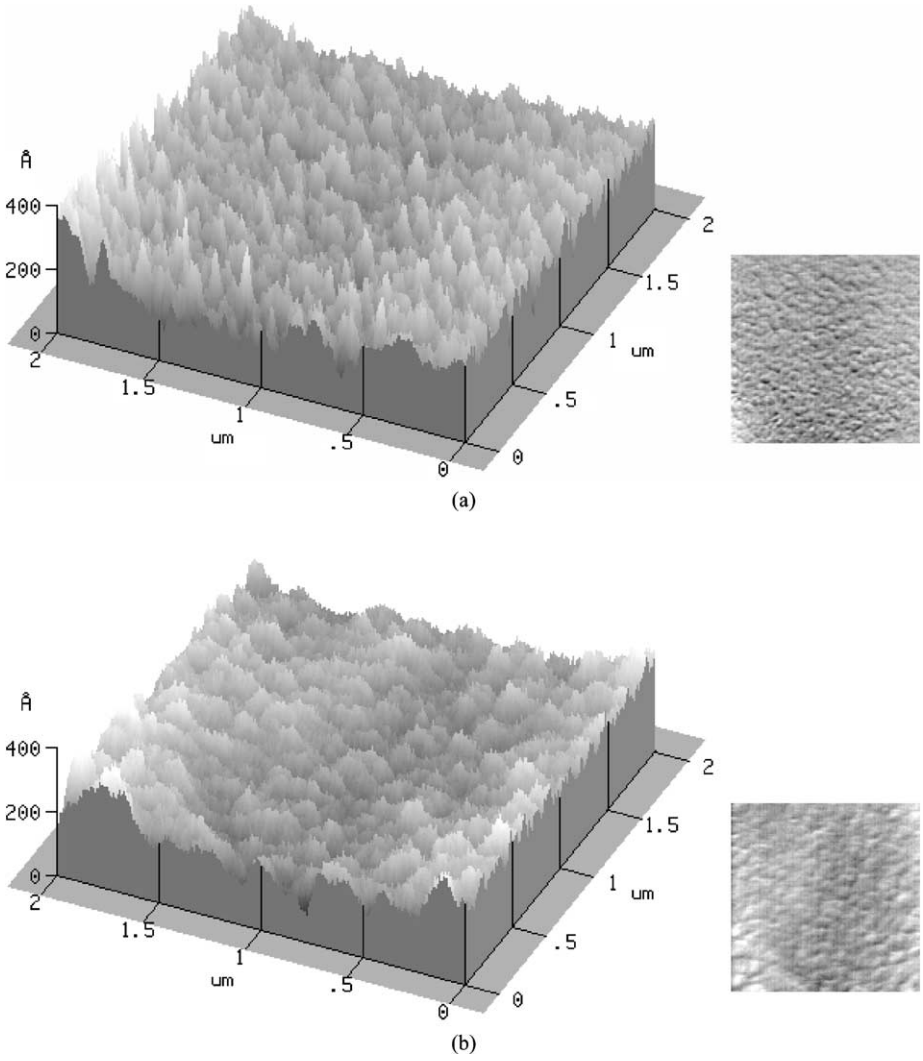

Fig. 3. AFM images of SiO_x layers of thickness: (a) 13 nm and (b) 43 nm. Only the upper surface of each sample is shown. The base of the vertical axis is arbitrary, i.e. it does not correspond to the polymer/oxide interface.

In contrast, a prior study reported partial coverage [1] of the substrate for very thin oxide layers. High resolution electron microscopy was unable to resolve any defect structure in the barrier coatings. This indicates that pores present were less than 1 nm in size. Selected area diffraction studies showed that the deposited SiO_x is amorphous. A detailed account of the film characterisation is given by Yanaka et al. [16].

4. Results and discussion

We have measured the permeability at 30 °C of several gases through PET (P_p) and PET/SiO_x films (P_b) as a function of glass thickness (13–67 nm). The results are shown in Table 3 and plotted in Fig. 4. Three samples of each barrier were analysed. In the table, we also report the ratio P_b/P_p, and the inferred glass permeability P_g. The latter quantity is calculated using ideal laminate theory under the assumption of negligible transport through macro-defects. The fact that P_b/P_p is not constant with thickness and permeant species rules out a picture where permeation is always dominated by macro-defects. Similarly, the fact that P_g decreases with thickness for helium, but increases for the other gases, rules out an ideal laminate model. If the film were an ideal laminate, P_g would have a constant value for each permeant, irrespective of thickness. The activation energy measurements for the noble gases are reported in Table 4. Since the trends in the data differ for each permeant species we discuss them separately.

Table 3
The measured permeability of films P_b coated with an evaporated silicon-oxide layer of thickness d_g (nm)

d_g	He			Ne			Ar			O_2		
	P_b	P_b/P_p	P_g	P_b	P_b/P_p	P_g	P_b	P_b/P_p	P_g	P_b	P_b/P_p	P_g
0	5.4E+05	1.000	–	65790	1.000	–	6304	1.000	–	7130	1.000	–
13	3.6E+05	0.674	1197	6518	0.099	0.06	315	0.050	0.36	337	0.047	0.38
23	1.9E+05	0.355	563	2255	0.034	0.21	256	0.041	0.50	224	0.031	0.44
43	8.9E+04	0.166	381	1836	0.028	0.56	273	0.043	0.99	179	0.025	0.65
67	4.4E+04	0.083	268	1591	0.024	1.18	324	0.051	1.78	173	0.024	0.98

The permeability of the oxide layer P_g is estimated using ideal laminate theory (Eq. (4)). The units used for permeability are 10^{-18} mol/(cm s atm).

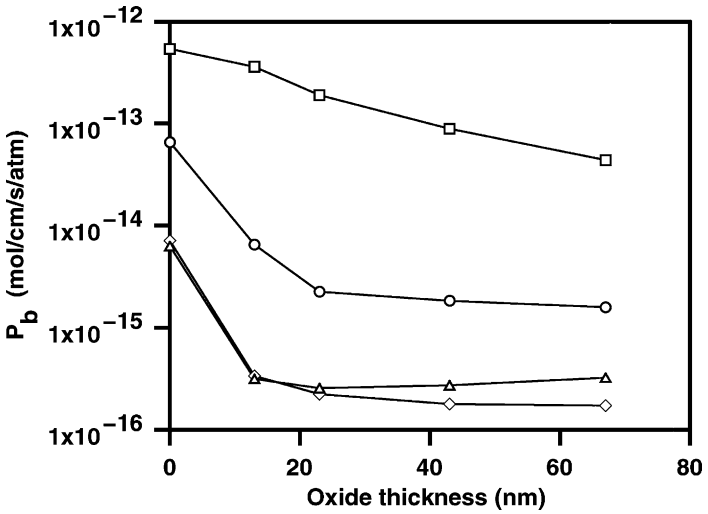

Fig. 4. Barrier permeability as a function of oxide thickness and permeant species: helium (□), neon (○), argon (△) and oxygen (◇).

Table 4
The activation energy ΔE (kJ/mol) of permeation for inert gases in films of varying oxide thickness

Gas	Bare PET	13 nm	43 nm
He	21	32	28
Ne	22	28	27
Ar	33	35	42

The value corresponds an average for three different samples. The sample variation is about ±5% of the reported average.

4.1. O_2

For oxygen permeation, it is believed that practically all the transport occurs through macro-defects [2], although for lower permeability films ($P_b/P_p \approx 0.004$), some role has been attributed to the SiO_x layer [6]. Assuming the oxygen permeates chiefly in molecular form (since atoms would be subject to severe chemical constraints), the lattice and nano-defects are simply to small to allow significant transport. This is useful as it allows us to determine $C_{md} = P_b/P_p \approx 0.04$. The same numerical value should apply to all other permeant species. Where $P_b/P_p > 0.04$, our model implies lattice or nano-defect permeation in addition to the macro-defect permeation reflected in C_{md}. For O_2, the value of C_{md} decreases slightly with thickness indicating, not surprisingly, that the density of macro-defects penetrating the whole thickness of the barrier layer decreases with oxide thickness. It is instructive to find values of the geometric parameters in Eq. (7) which are consistent with $C_{md} \approx 0.04$. Some examples are given in Table 5. If the macro-defects are small (width 75 nm), they only need occupy 0.001% of the overall oxide surface. The implied rarity of the defects may explain why we have observed no macro-defects in our characterisation studies.

Table 5
Using Eq. (7), we have calculated hypothetical sizes ($W = 2w$) and spacings (L) of macro-defects which are consistent with the observed defect permeability ($C_{md} \approx 0.04$)

W (μm)	L (μm)	Area fraction (W^2/L^2)
0.075	2	1.4×10^{-5}
0.03	4	5.6×10^{-5}
0.12	8	2.3×10^{-4}
0.47	16	8.8×10^{-4}
1.85	32	3.3×10^{-3}

Previous experiments using plasma enhanced CVD to deposit SiO_x on polycarbonate have reported activation energies for permeation which differ from the those obtained for the polymer alone [6]. Prior to deposition $\Delta E_p = 17$ kJ/mol and $P_p \approx 764$ kp.u. (910 cm^3/m^2 per day/atm × 0.18 mm). With a deposition thickness of $t = 100$ nm the barrier properties were $\Delta E_b \approx 25$ kJ/mol, and $P_b = 1.7$ kp.u. (2 cm^3/m^2 per day/atm × 0.18 mm). Since $\Delta E_b > \Delta E_p$ the authors concluded that diffusion was SiO_x limited, i.e. $C_{md} = 0$. Assuming $P_{la} = 0$, Eq. (11) can be solved to give $P_{nd} = 0.93$ p.u. Comparing ΔE_b and P_{nd} to the data in Table 1, the glass layer is similar in performance to K-mordenite with 0.4 nm pores. The inferred pore size is 20% smaller than the previously estimated value [6]. Their value (around 0.5–0.6 nm) is based on the assumption that only the difference in activation energy between the polymer and laminate barrier $\Delta E_b - \Delta E_p \approx 25 - 17 = 8$ kJ/mol (up to a value of 17 kJ/mol, depending on the particular barrier) corresponds to the activation energy of the glass. Instead, we used the more appropriate assumption $\Delta E_b \approx \Delta E_g$ based on Eq. (3).

4.2. Inert gases

For argon permeation, we find P_b/P_p is slightly higher (25%) than C_{md} for O_2 permeation. This may indicate some permeation is actually occurring through the solid SiO_x layer. This is supported by the activation energy of permeation ($\Delta E_b = 35$ and 42 kJ/mol at 13 and 43 nm) being slightly greater than $\Delta E_p = 33$ kJ/mol. This activation energy is far less than that expected for argon diffusion through the lattice of annealed silicon oxide (105 kJ/mol), but is consistent with diffusion through the 0.4 nm pathways of K-mordenite, which corresponds to the proposed size of the nano-defects in our model.

For helium P_b/P_p is significantly greater than C_{md} for O_x permeation and $\Delta E_b > \Delta E_p$. This indicates that the majority of transport is limited by the SiO_x layer. The inferred permeability of the glass ($P_g = 1197$ p.u. at 13 nm), and activation energy $\Delta E_b = 32$ kJ/mol are consistent with lattice diffusion in glass with structure between that of annealed silicon oxide (20 kp.u., $\Delta E_g = 21$ kJ/mol) and soda lime glass (2.3 p.u., $\Delta E_g = 46$ kJ/mol). This suggests that the oxide lattice interstices are similar in size to silica

glass (0.27 nm). Using $C_{md} = 0.04$, we infer that of the total helium permeation $P_b = 360$ kp.u., a portion equal to $0.04 \times P_p = 22$ kp.u. is actually migrating un-hindered through the defects. Since this represents only 6% of the total flux, the majority of flux, and hence activation energy, is controlled by the oxide lattice. As the glass layer increases in thickness, the total barrier permeability decreases, so the proportion of flux passing through macro-defects increases. For example, at thickness $d_g = 43$ nm, $P_b = 89$ kp.u., indicating nearly 25% of the total flux is expected to pass unhindered through macro-defects. The decrease in activation energy from 32 to 28 kJ/mol is consistent with this inference.

For neon permeation through the barrier film with an oxide coating of 13 nm, the expected macro-defect contribution is 0.04×66 kp.u. $= 2.6$ kp.u., which is around half that observed $P_b = 6.5$ kp.u. The conclusion that gas is permeating in the oxide later is supported by the observation that $\Delta E_g = 28$ kJ/mol is indeed greater than $\Delta E_p = 22$ kJ/mol. Using Eq. (11) we calculate $P_g = 3.6$ p.u. This is only slightly less than 4.6 p.u. ($\Delta E_g = 48$ kJ/mol) for lattice permeation in annealed silicon oxide with 0.27 nm interstices, but our measured activation energy is lower indicating that the pores through which neon pass have a diameter greater than 0.27 nm. Note that zeolite KA with 0.3 nm pores has $\Delta E = 29$ kJ/mol, closer to our measured value. Therefore, neon permeation may be occurring through nano-defects of around 0.3 nm in size. The defects are only slightly larger than the 0.27 nm lattice interstices of solid oxide through which the helium gas migrates.

4.3. H_2O

Tropsha and Harvey [2] measured H_2O and O_2 permeation of SiO_x coated polymer films (mainly PET), the silicon oxide layer deposited by plasma enhanced chemical vapour deposition (CVD). For our purposes, their key experimental findings were as follows. For oxygen permeation $P_b/P_p = 0.005$–0.010 (average 0.006), but $P_b/P_p = 0.036$–0.14 (average 0.07) for H_2O permeation. Also, $\Delta E_p \approx \Delta E_b \approx 30$ kJ/mol for O_2, but $\Delta E_b \approx 55$ kJ/mol for H_2O, independent of four different polymer substrates (with $\Delta E_p =$ 23–55 kJ/mol). The O_2 data support a macro-defect picture [2], but the activation energy of H_2O transport appears to indicate that the H_2O molecules diffuse through the glass. Tropsha and Harvey [2] rule out the latter hypothesis on the basis that (i) $\Delta E_b \approx 55$ kJ/mol $\ll 84$ kJ/mol for water in glass [12] and (ii) they assumed that the water would not permeate through the glass lattice at room temperature (based on high temperature data). Earlier we showed that these assumptions are not necessarily true. The presence of nano-defects in the glass can halve the activation energy, and increase the expected diffusion coefficient by four orders of magnitude [12].

It is, therefore, interesting to ask if Tropsha and Harvey's data can be reinterpreted using the purely physical model (i.e. for chemically inert gases) proposed here. Given the relatively large size of a water molecule (0.33 nm) we assume that practically all the diffusion is through nano-defects (so $P_{la} \approx 0$). For the barrier of Tropsha and Harvey we have all the variables in Eq. (11) bar P_{nd}, which can be calculated. From [2] we have $d_g = 100$ nm, $d_p = 25$ μm, $P_b = 4.95 \times 10^5$ p.u. (19.77×10^{-7} mol/(m^2 s) $\times$ 25 μm), $P_p = 5.3 \times 10^6$ p.u. (212×10^{-7} mol/(m^2/s) $\times$ 25 μm). From $P_b/P_p = 0.006$ for O_2 we infer $C_{md} = 0.006$, which implies $P_{nd} = 2$ kp.u. This is still six orders of magnitude greater than the independently determined value for silica glass (0.0029 p.u. in Table 1). Under the assumption of molecular transport, this implies that there are many more nano-defects in CVD SiO_2 than silica glass. Since little data for H_2O diffusion in materials other than glass is available it is hard to estimate the nano-defect size from the measured activation energy (55 kJ/mol). Given that the diameter of H_2O (0.33 nm) is slightly larger than argon (3.2 nm) we estimate a nano-defect size of 0.3–0.4 nm from Table 1. Our interpretation of H_2O permeation data is speculative only. There are a range of factors [2,10–12] which complicate water permeation in glass (such as chemical interactions), although it has also been suggested that diffusion of molecular water predominates transport [23].

5. Conclusion

We have proposed a quantitative model for permeation in SiO_x/polymer barrier films which takes into account permeation through the lattice ('pore' size <0.3 nm), nano-defects (0.3–1.0 nm), and

macro-defects (>1 nm) of the oxide layer. It is necessary to postulate the presence of nano-defects in the oxide layer to explain experimental data which neither fits the ideal laminate hypothesis or a purely macro-defect model. Evidence of nano-defects in silica glasses has been previously found based on observed decreases in the activation energy of permeation at low temperatures [8,12]. The role of nano-defects will be especially pronounced for relatively large molecules (e.g. O_2 and H_2O) since their lattice permeabilities (extrapolated from high temperature studies) at room temperature are virtually negligible.

To gauge the size of the nano-defects we have collated data on well characterised solids with 'pore' sizes ranging from 0.27 to 0.6 nm. Therefore, the 'pore' size in oxide coatings can be inferred by comparing the measured activation energy with tabulated values. This is possible if a portion of the total permeation is traversing the oxide layer; if macro-defects dominate, the solid oxide layer will be bypassed. Using the quantitative model (Eq. (11)) it is also possible to obtain a direct estimate of the oxide permeability. In order to relate the study of barrier films to other work in the literature, it is important to express the barrier properties in terms of the more fundamental quantities of permeability, diffusivity and solubility. We have provided rough estimates of the solubility for inert gases and H_2O, but specific values for barrier materials would be desirable.

We have used the model to interpret permeation of helium, neon, and argon through electron beam evaporated SiO_x/PET barriers of varying thickness. The data cannot be explained by an ideal laminate or a macro-defect theory alone. Oxygen permeation experiments indicate the presence of macro-defects, but our model for macro-defect permeation indicates that the defects could be both small and rare. This provides an explanation of why they cannot be detected even in thorough characterisation studies (e.g. Section 3.3).

Our permeation results indicate that helium passes through the oxide lattice and macro-defects of electron beam evaporated SiO_x. The measured activation energy and inferred glass permeability imply the lattice interstices are slightly smaller than those found in annealed silicon oxide. The activation energy of neon permeation is significantly smaller than expected for annealed silicon oxide. This indicates that neon atoms traverse slightly larger nano-defects (≈0.3 nm) in addition to the macro-defects. The activation energy of argon permeation implies the existence of still larger nano-defects (≈0.4 nm). Of course helium and neon will also pass through these defects, but the majority of the flux in each case will be dominated by the smaller (more common) nano-defects or lattice interstices. Consideration of prior O_2 permeation experiments [6] in terms of our model also implied that larger molecules permeate through ≈0.4 nm nano-defects.

References

[1] J.T. Felts, Thickness effects on thin film gas barriers: silicon-based coatings, in: Proceedings of the 34th Annual Technical Conference, Society of Vacuum Coaters, 1991, p. 99.

[2] Y.G. Tropsha, N.G. Harvey, Activated rate theory treatment of oxygen and water transport through silicon oxide/poly(ethylene terephtalate) composite barrier structures, J. Phys. Chem. B 101 (1997) 2259.

[3] J.D. Affinito, et al., Polymer-oxide transparent barrier layers, in: Proceedings of the 39th Annual Technical Conference, Paper W-12, Society of Vacuum Coaters, 1997.

[4] F.J. Norton, Permeation of gaseous oxygen through vitreous silica, Nature 191 (1961) 701.

[5] J. Moulson, J.P. Roberts, Water in silica glass, Trans. Faraday Soc. 57 (1961) 1208.

[6] A.G. Erlat, B.C. Wang, R.J. Spontak, Y. Tropsha, K.D. Mar, D.B. Montgomery, E.A. Vogler, Morphology and gas barrier properties of thin SiO_x coatings on polycarbonate: correlations with plasma enhanced chemical vapour deposition conditions, J. Mater. Res. 15 (2000) 704.

[7] A.G. Erlat, R.J. Spontak, R.P. Clarke, T.C. Robinson, P.D. Haaland, Y. Tropsha, N.G. Harvey, E.A. Vogler, SiO_x gas barrier coatings on polymer substrates: morphology and gas transport considerations, J. Phys. Chem. B 103 (1999) 6047.

[8] R.M. Barrer, Diffusion In and Through Solids, Cambridge University Press, Cambridge, 1941.

[9] J. Crank (Ed.), Diffusion in Polymers, Academic Press, London, 1968.

[10] J.E. Shelby, Handbook of Gas Diffusion in Solids and Melts, ASM International, Materials Park, OH, 1996.

[11] R.H. Doremus, Glass Science, Wiley, New York, 1973.

[12] H. Wakabayashi, M. Tomozawa, Diffusion of water into silica glass at low temperature, J. Am. Ceram. Soc. 72 (1989) 1850.

[13] Y. Zhang, H_2O solubility in rhyolitic glasses and melts: measurement, speciation, solubility and diffusion, Rev. Geophys. 37 (1999) 493.

[14] G. Rossi, M. Nulman, Effect of local flaws in polymeric permeation reducing barriers, J. Appl. Phys. 74 (1993) 5471.

[15] A.P. Roberts, et al., Gas diffusion through laminate films containing defects, In preparation.

[16] M. Yanaka, B.M. Henry, A.P. Roberts, C.R.M. Grovenor, G.A.D. Briggs, A.P. Sutton, T. Miyamoto, Y. Tsukahara, N. Takeda, R.J. Chater, How cracks in SiO_x-coated polyester films affect gas permeation, Thin Solid Films 397 (2001) 176.

[17] F.J. Norton, Helium diffusion through glass, J. Am. Ceram. Soc. 36 (1953) 90.
[18] W.G. Perkins, D.R. Begeal, Diffusion and permeation of He, Ne, Ar, Kr, and D_2 through silicon oxide thin films, J. Chem. Phys. 54 (1971) 1683.
[19] V. Stannett, in: J. Crank (Ed.), Diffusion in Polymers, Academic Press, London, 1968 (Chapter 2).
[20] J.A. Slee, et al., The transport of oxygen through oriented poly(ethylene terephtalate), J. Polym. Sci. B 27 (1989) 71.
[21] A.B. Shelekhin, A.G. Dixon, Y.H. Ma, Theory of gas diffusion and permeation in inorganic molecular sieve membranes, AIChE J. 41 (1995) 58.
[22] W.G. Pollard, R.D. Present, On gaseous self-diffusion in long capillary tubes, Phys. Rev. 73 (1948) 762.
[23] Y. Guissani, B. Guillot, Transport of rare gases and molecular water in fused silica by molecular dynamics simulation, Mol. Phys. 95 (1998) 151.
[24] R.M. Barrer, Zeolites and Clay Minerals as Sorbents and Molecular Sieves, Academic Press, London, 1978.
[25] P.S. Holden, G.A.J. Orchard, I.M. Ward, A study of the gas barrier properties of highly oriented polyethylene, J. Polym. Sci., Polym. Phys. Ed. 23 (1985) 709.
[26] G.A.J. Orchard, P. Spiby, I.M. Ward, Oxygen and water-vapour diffusion through bi-axially oriented poly(ethylene terephtalate), J. Polym. Sci. B 28 (1990) 603.